Theory of nonlinear cyclotron resonance in quasi-two-dimensional electron systems

2003 J. Phys.: Condens. Matter 15 4411

(http://iopscience.iop.org/0953-8984/15/25/311)

INSTITUTE OF PHYSICS PUBLISHING JOURNAL OF PHYSICS: CONDENSED MATTER

J. Phys.: Condens. Matter **15** (2003) 4411–4427 PII: S0953-8984(03)60526-6

Theory of nonlinear cyclotron resonance in quasi-two-dimensional electron systems

S Y Liu[1] **and X L Lei**

Department of Physics, Shanghai Jiaotong University, 1954 Huashan Road, Shanghai 200030, China

E-mail: liusy@mail.sjtu.edu.cn

Received 6 March 2003
Published 13 June 2003
Online at stacks.iop.org/JPhysCM/15/4411

Abstract

Momentum- and energy-balance equations are developed for steady-state electron transport and optical absorption under the influence of a dc electric field and an intense ac electric field of terahertz (THz) frequency in a two-dimensional (2D) semiconductor in the presence of a strong magnetic field perpendicular to the 2D plane. These equations are applied to study the intensity-dependent cyclotron resonance (CR) in far-infrared transmission and THz-radiation-induced photoconductivity of GaAs heterostructures in the Faraday geometry. We find that the CR peaks and line shapes of the transmittance exhibit different intensity dependences when the intensity of the THz field increases in the ranges above or below a certain critical value. The CR in the photoresistivity, however, is always enhanced on increasing the intensity of the THz field. These results agree qualitatively with the experimental observations. We have clarified that the CR in the photoconductivity is not only a result of the electron heating, but also arises from photon-assisted scattering enhancement, especially at high temperatures. The effects of an intense THz field on the Faraday angle and ellipticity of magnetically biased 2D semiconductors have also been demonstrated.

1. Introduction

Cyclotron resonance (CR) is a fundamental process for carriers in quasi-two-dimensional semiconductors subjected simultaneously to a magnetic field and a far-infrared or terahertz (THz) ac field. It occurs when the separation between two adjacent Landau levels is close to the photon energy of the ac field, and leads to resonant behaviour in the absorption and in the photoconductivity as functions of the magnetic field.

[1] Author to whom any correspondence should be addressed.

0953-8984/03/254411+17$30.00

CR in absorption or transmission has been proved to be a powerful tool providing valuable information for two-dimensional (2D) semiconductors on the carrier scattering processes, the confining potential, and even the spin relaxation mechanisms [1]. Generally, weak far-infrared irradiations were used in most experiments, and theoretical analyses focused on the linear response of the system to the ac field [2]. When the strength of the incident radiation field increased, nonlinear behaviour of the CR in absorption and transmission was observed. It was found [3] that the resonant-field-to-zero-field transmissivity ratio reduced slightly with increase in intensity of the far-infrared field from 0.1 W cm^{-2}, then increased for radiation field intensities above 10 W cm^{-2}. This kind of intensity-dependent CR transmission has not yet been explained, except by a simple comparison with a linear response formula of Drude type taking the scattering time as a fitting parameter.

Another manifestation of CR shows up in photoresponses, namely, photoconductivity or photoresistivity. The latter is defined as the longitudinal dc magnetoresistivity change induced by the irradiation of the high-frequency electromagnetic wave, which exhibits a resonant peak structure under CR condition. This effect has long been known at low temperatures, and was believed to arise from the electron-heating-induced redistribution of the electron gas upon absorbing the radiation field energy [4, 5]. The energy absorption and thus the rise of the electron temperature exhibit maxima when the photon energy of the radiation field equals the cyclotron energy, yielding the resonance peak structure of the photoresistivity. Later analysis of experimental data [6] indicated that, in addition to this heating-induced electron redistribution, another nonthermal mechanism might be needed to account for the observed photoconductivity of GaAs/AlGaAs heterostructures at CR. Recent photoresistivity measurements on a GaAs/AlGaAs heterojunction performed at the lattice temperature $T = 150$ K with exposure to irradiation of 4 THz frequency [7] surprisingly showed remarkable CR peaks. At such a high lattice temperature with strong polar optic phonon scattering providing an efficient energy dissipation channel, the radiation-induced electron temperature increase is far smaller, to account for such strong CR in photoresistivity. So far no convincing nonthermal mechanism responsible for far-infrared photoconductivity in semiconductors has been proposed. A nonlinear theory for high-temperature photoresistivity CR in two-dimensional systems is still lacking. It is an urgent need to develop a tractable, microscopic theory capable of treating nonlinear absorption and photoresponse under intense THz radiation and to clarify the lacking nonthermal mechanism for high-temperature photoresistivity in two-dimensional semiconductors.

A few years ago, one of the authors developed a balance-equation approach [8] for hot-electron transport driven by a THz electric field of single frequency ($\boldsymbol{E}_\omega \sin(\omega t)$). This method made use of the fact that, when the harmonic generation is small and the frequency gets into the THz regime or higher, the electron drift velocity in the steady transport state oscillates almost out of phase with the electric field, i.e. the drift velocity is essentially of the form $\boldsymbol{v}_1 \cos(\omega t)$. At the same time, all orders of these (frequency ω) photon-assisted impurity and phonon scatterings are included in the relaxation processes. This method has been successfully applied in discussing the THz photoabsorption and THz-induced dc conductivity response in bulk and two-dimensional semiconductors in the case without magnetic field [8, 9] or with a magnetic field in the Voigt configuration [10]. However, this assumption of such a time-dependent form of the drift velocity will no longer hold when there is a strong magnetic field $\boldsymbol{B}$ not parallel to $\boldsymbol{v}_1$. Since the Lorentz force $e\boldsymbol{v}_1 \times \boldsymbol{B}\cos(\omega t)$ acts on the moving electron, its steady-state drift velocity will contain a term $(\omega_c/\omega)v_1 \sin(\omega t)$, where $\omega_c = |eB|/m$ is the cyclotron frequency. This velocity, which is perpendicular to $\boldsymbol{v}_1$ and $\boldsymbol{B}$, and oscillates $\pi/2$ out of phase with $\boldsymbol{v}_1 \cos(\omega t)$, is of the same order of magnitude as $\boldsymbol{v}_1$ in the frequency and magnetic field range $\omega \sim \omega_c$. Because of this, the balance-equation method used in [10] is not able to deal with the problem related to CR in semiconductors in the Faraday geometry.

The purpose of this paper is to develop a theory for electron transport driven by an intense far-infrared electric field in a quasi-2D semiconductor in the presence of an arbitrary magnetic field perpendicular to the 2D plane. We find that it is possible to extend the balance-equation method proposed in [8] to the case in the presence of a quantized magnetic field in the Faraday configuration, and to deal with problems in magnetotransport, such as the intensity-dependent THz transmission and the photoresponse at CR in quasi-2D electron systems.

This paper is organized as follows. In section 2 we will sketch the derivation of the force- and energy-balance equations for quasi-two-dimensional electron systems subjected to a magnetic field, and arbitrary dc and THz ac electric fields. In section 3 the CR in time-dependent drift velocity is discussed. The investigations of CR in transmission and photoconductivity are presented, respectively, in sections 4 and 5. Finally, in section 6 a short conclusion will be given.

2. Formulation

2.1. Hamiltonian

We consider N_e electrons in a unit area of a quasi-two-dimensional system, such as a heterojunction or a quantum well. In these systems the electrons are free to move in the x–y plane, but are subjected to a confining potential $V(z)$ in the z-direction. These electrons are interacting with each other and also coupled with phonons and scattered by randomly distributed impurities in the lattice.

To include possible elliptically polarized electromagnetic radiation we assume that a uniform dc electric field $\boldsymbol{E}_0$ and a THz ac field $\boldsymbol{E}(t)$ of angular frequency ω,

$$\boldsymbol{E}(t) \equiv \boldsymbol{E}_s \sin(\omega t) + \boldsymbol{E}_c \cos(\omega t), \tag{1}$$

are applied in the x–y plane, together with a uniform magnetic field $\boldsymbol{B} = (0, 0, B)$ along the z-axis. These magnetic and electric fields can respectively be described by a vector potential $\boldsymbol{A}(\boldsymbol{r})$ and a scalar potential $\varphi(\boldsymbol{r}, t)$ of the form

$$\boldsymbol{\nabla} \times \boldsymbol{A}(\boldsymbol{r}) = \boldsymbol{B}, \tag{2}$$

$$\varphi(\boldsymbol{r}, t) = -\boldsymbol{r} \cdot \boldsymbol{E}_0 - \boldsymbol{r} \cdot \boldsymbol{E}(t). \tag{3}$$

In the presence of these electric and magnetic fields the Hamiltonian of the system has the form

$$H = H_{eE}(t) + H_{ei} + H_{ep} + H_{ph}. \tag{4}$$

Here,

$$H_{eE}(t) = \sum_j \left[\frac{1}{2m}(\boldsymbol{p}_{j\|} - e\boldsymbol{A}(\boldsymbol{r}_{j\|}))^2 + \varphi(\boldsymbol{r}_{j\|}, t) + \frac{p_{jz}^2}{2m_z} + V(z_j) \right] + \sum_{i<j} V_c(\boldsymbol{r}_{i\|} - \boldsymbol{r}_{j\|}, z_i, z_j) \tag{5}$$

is the Hamiltonian of electrons driven by the electric and magnetic fields with V_C being the electron–electron Coulomb interaction; H_{ei} and H_{ep} are, respectively, the electron–impurity and electron–phonon couplings. In equation (5), $\boldsymbol{r}_{j\|} \equiv (x_j, y_j)$ and $\boldsymbol{p}_{j\|} \equiv (p_{jx}, p_{jy})$ are the coordinate and momentum of the jth electron in the 2D plane, and z and p_{jz} are those perpendicular to the plane; m and m_z are, respectively, the effective mass parallel and perpendicular to the plane.

It is convenient to introduce two-dimensional centre-of-mass momentum and coordinate variables $\boldsymbol{P} \equiv (P_x, P_y)$ and $\boldsymbol{R} \equiv (R_x, R_y)$:

$$\boldsymbol{P} = \sum_j \boldsymbol{p}_{j\parallel}, \qquad \boldsymbol{R} = \frac{1}{N_e}\sum_j \boldsymbol{r}_{j\parallel} \tag{6}$$

and the relative electron momentum and coordinate variables $\boldsymbol{p}'_j \equiv (\boldsymbol{p}'_{j\parallel}, p_{jz})$ and $\boldsymbol{r}' = (\boldsymbol{r}'_{j\parallel}, z_j)(j = 1, \ldots, N_e)$:

$$\boldsymbol{p}'_{j\parallel} = \boldsymbol{p}_{j\parallel} - \frac{1}{N_e}\boldsymbol{P}, \qquad \boldsymbol{r}'_{j\parallel} = \boldsymbol{r}_{j\parallel} - \boldsymbol{R}. \tag{7}$$

In terms of these variables, the Hamiltonian H_{eE} can be separated into a centre-of-mass part H_{cm} and a relative electron part H_{er}:

$$H_{eE} = H_{cm} + H_{er}, \tag{8}$$

$$H_{cm} = \frac{1}{2N_e m}(\boldsymbol{P} - N_e e\boldsymbol{A}(\boldsymbol{R}))^2 - N_e e\boldsymbol{E}_0 \cdot \boldsymbol{R} - N_e e\boldsymbol{E}(t) \cdot \boldsymbol{R}, \tag{9}$$

$$H_{er} = \sum_j \left[\frac{1}{2m}(\boldsymbol{p}'_{j\parallel} - e\boldsymbol{A}(\boldsymbol{r}'_{j\parallel}))^2 + \frac{p_{jz}^2}{2m_z} + V(z_j)\right] + \sum_{i<j} V_C(\boldsymbol{r}'_{i\parallel} - \boldsymbol{r}'_{j\parallel}, z_i, z_j). \tag{10}$$

It should be noted that the relative electron Hamiltonian H_{er} is the just that of a quasi-2D system subjected to a uniform magnetic field in the z-direction. Its eigenstate can be designated by a subband index s, a Landau-level index n, and a wavevector k_y, having the energy spectrum

$$\varepsilon_{sn} = \varepsilon_s + (n - \tfrac{1}{2})\omega_c, \qquad s = 0, 1, \ldots \text{ and } n = 1, 2, \ldots, \tag{11}$$

where $\omega_c = |eB|/m$ is the cyclotron frequency. In this paper we will limit consideration to the case where the 2D electrons occupy only the lowest subband and ignore index s. In equation (5) the electron–impurity and electron–phonon interactions H_{ei} and H_{ep} have the same expressions as those given in [11], in terms of centre-of-mass coordinate $\boldsymbol{R}$ and the density operator of the relative electrons,

$$\rho_{\boldsymbol{q}_\parallel} = \sum_j \mathrm{e}^{\mathrm{i}\boldsymbol{q}_\parallel \cdot \boldsymbol{r}'_j}. \tag{12}$$

2.2. Balance equations

On the basis of the Heisenberg equation of motion we can derive the velocity (operator) of the centre of mass, $\boldsymbol{V}$, which is the rate of change of the centre-of-mass coordinate $\boldsymbol{R}$, and equation for the rate of change of the centre-of-mass velocity $\boldsymbol{V} \equiv \dot{\boldsymbol{R}}$:

$$\boldsymbol{V} = -\mathrm{i}[\boldsymbol{R}, H] = \frac{1}{N_e m}(\boldsymbol{P} - N_e e\boldsymbol{A}(\boldsymbol{R})), \tag{13}$$

and

$$\dot{\boldsymbol{V}} = -\mathrm{i}[\boldsymbol{V}, H] + \frac{\partial \boldsymbol{V}}{\partial t} = \frac{e}{m}\{\boldsymbol{E}_0 + \boldsymbol{E}(t) + \boldsymbol{V} \times \boldsymbol{B}\} + \frac{\boldsymbol{F}}{N_e m}, \tag{14}$$

with

$$\boldsymbol{F} = -\mathrm{i}\sum_{\boldsymbol{q}_\parallel, a} U(\boldsymbol{q}_\parallel, z_a)\boldsymbol{q}_\parallel \mathrm{e}^{\mathrm{i}\boldsymbol{q}_\parallel \cdot (\boldsymbol{R} - \boldsymbol{r}_a)}\rho_{\boldsymbol{q}_\parallel} - \mathrm{i}\sum_{\boldsymbol{q},\lambda} M(\boldsymbol{q}, \lambda)\phi_{\boldsymbol{q}\lambda}\mathrm{e}^{\mathrm{i}\boldsymbol{q}_\parallel \cdot \boldsymbol{R}}\rho_{\boldsymbol{q}_\parallel}. \tag{15}$$

We can also derive the equation for the rate of change of the relative electron energy:

$$\dot{H}_{er} = -\mathrm{i}[H_{er}, H] = -\mathrm{i}\sum_{\boldsymbol{q}_\parallel, a} U(\boldsymbol{q}_\parallel, z_a)\mathrm{e}^{\mathrm{i}\boldsymbol{q}_\parallel \cdot (\boldsymbol{R} - \boldsymbol{r}_a)}\dot{\rho}_{\boldsymbol{q}_\parallel} - \mathrm{i}\sum_{\boldsymbol{q},\lambda} M(\boldsymbol{q}, \lambda)\phi_{\boldsymbol{q}\lambda}\mathrm{e}^{\mathrm{i}\boldsymbol{q}_\parallel \cdot \boldsymbol{R}}\dot{\rho}_{\boldsymbol{q}_\parallel}. \tag{16}$$

In equations (15), (16) $(\boldsymbol{r}_a, z_a)$ and $U(\boldsymbol{q}_\parallel, z_a)$ are the impurity position and its potential, $M(\boldsymbol{q}, \lambda)$ is the matrix element due to coupling between electrons and a phonon of wavevector $\boldsymbol{q} \equiv (\boldsymbol{q}_\parallel, q_z)$ in branch λ having energy $\Omega_{\boldsymbol{q}\lambda}$, $\phi_{\boldsymbol{q}\lambda} \equiv b_{\boldsymbol{q}\lambda} + b^\dagger_{-\boldsymbol{q}\lambda}$ stands for the phonon field operator, and $\dot{\rho}_{\boldsymbol{q}_\parallel} \equiv -\mathrm{i}[\rho_{\boldsymbol{q}_\parallel}, H_{er}]$.

In order to derive the force- and energy-balance equations we need to carry out the statistical averaging of these operator equations. As proposed in [12], we treat the centre-of-mass coordinate $\boldsymbol{R}$ and velocity $\boldsymbol{V}$ classically, and by neglecting their small fluctuations we will regard them as time-dependent expectation values of the centre-of-mass coordinate and velocity, $\boldsymbol{R}(t)$ and $\boldsymbol{V}(t)$. In the present paper, we are mainly concerned with the steady transport state under a THz irradiation of single frequency and focus on the photoresponse of the dc conductance and the energy absorption and transmission of the THz signal. These quantities are directly related to the time-averaged and base frequency oscillating components of the centre-of-mass velocity. The second- and higher-harmonic components of the electron velocity, if any, though giving no direct contribution to ac field transmission and dc photoresponse, would enter the frictional force, energy transfer, and energy absorption rates in the resulting equations, and thus may in turn affect the time-averaged and lower-harmonic terms of the drift velocity. However, unless in a specially designed system, the generated power of the third-harmonic current in an ordinary semiconductor is generally less than a few per cent of the base frequency power even in the case of strongly nonlinear transport when the ac field amplitude gets as high as several kilovolts per centimetre or higher [13, 14]. Its effect on the photon-assisted scattering matrix element will be an order of magnitude weaker than that of the base frequency photons [8–10]. For the radiation field intensity concerned in the present study, which is an order of magnitude smaller than that for the above-mentioned harmonic generation, the effect of higher-harmonic current is safely negligible. Hence, it suffices to assume that the centre-of-mass velocity, i.e. the electron drift velocity, consists of only a dc part $\boldsymbol{v}_0$ and a stationary time-dependent part $\boldsymbol{v}(t)$ of the form

$$\boldsymbol{V}(t) = \boldsymbol{v}_0 + \boldsymbol{v}_1 \cos(\omega t) + \boldsymbol{v}_2 \sin(\omega t). \tag{17}$$

On the other hand, in order to carry out the statistical averaging we need the density matrix $\hat{\rho}$. For 2D systems having electron sheet densities of the order of, or higher than, 10^{15} m^{-2}, the intrasubband and intersubband Coulomb interactions are sufficiently strong that it is adequate to describe the relative electron transport state using a single electron temperature T_e. Hence, the density matrix can be obtained from solving the Liouville equation by starting from the initial state of the relative electron–phonon system at time $t = -\infty$, in which the phonon system is in equilibrium at lattice temperature T and the relative electron system is in equilibrium at an electron temperature T_e:

$$\hat{\rho}|_{t=-\infty} = \hat{\rho}_0 = \frac{1}{Z} \mathrm{e}^{-H_{er}/T_e} \mathrm{e}^{-H_{ph}/T} \tag{18}$$

where Z is the normalized parameter.

With the density matrix thus obtained to the first order in $H_{ei} + H_{ep}$, we can carry out the statistical averaging of operator equations (14) and (16). In the procedure, the form factor

$$\begin{aligned} A(\boldsymbol{q}, t, t') \equiv \mathrm{e}^{-\mathrm{i}\boldsymbol{q}\cdot\int_{t'}^{t} \boldsymbol{v}(s)\,\mathrm{d}s} &= \sum_{n=-\infty}^{\infty} J_n^2(\xi) \mathrm{e}^{\mathrm{i}(\boldsymbol{q}\cdot\boldsymbol{v}_0 - n\omega)(t-t')} \\ &+ \sum_{m\neq 0} \mathrm{e}^{\mathrm{i}m(\omega t - \varphi)} \left[\sum_{n=-\infty}^{\infty} J_n(\xi) J_{n-m}(\xi) \mathrm{e}^{\mathrm{i}(\boldsymbol{q}\cdot\boldsymbol{v}_0 - n\omega)(t-t')} \right] \end{aligned} \tag{19}$$

is expanded in terms of the Bessel functions $J_n(x)$. Here $\xi \equiv \sqrt{(\boldsymbol{q}_\parallel \cdot \boldsymbol{v}_1)^2 + (\boldsymbol{q}_\parallel \cdot \boldsymbol{v}_2)^2}/\omega$ and φ satisfies the relation $\tan\varphi = (\boldsymbol{q}\cdot\boldsymbol{v}_2)/(\boldsymbol{q}\cdot\boldsymbol{v}_1)$.

Since all the transport properties are measured over a time interval much longer than the period of the THz field and we are concerned only with photoresponse and photoabsorption of the system, it suffices for us to know the frictional force for the time oscillating term with base frequency ω and the energy-related quantity for the time-averaged term. The frictional force can be written as

$$\boldsymbol{F}(t) = \boldsymbol{F}_0 - (\boldsymbol{F}_{11} - \boldsymbol{F}_{22})\sin(\omega t) + (\boldsymbol{F}_{12} + \boldsymbol{F}_{21})\cos(\omega t), \tag{20}$$

with the functions $\boldsymbol{F}_0$ and $\boldsymbol{F}_{\mu\nu}$ ($\mu, \nu = 1, 2$) given by

$$\boldsymbol{F}_0 = \sum_{\boldsymbol{q}_\parallel} \boldsymbol{q}_\parallel |U(\boldsymbol{q}_\parallel)|^2 \sum_{n=-\infty}^{\infty} J_n^2(\xi)\Pi_2(\boldsymbol{q}_\parallel, \omega_0 - n\omega) + \sum_{\boldsymbol{q},\lambda} \boldsymbol{q}_\parallel |M(\boldsymbol{q}, \lambda)|^2 \sum_{n=-\infty}^{\infty} J_n^2(\xi)\Lambda_2(\boldsymbol{q}, \lambda, \omega_0 + \Omega_{\boldsymbol{q}\lambda} - n\omega), \tag{21}$$

$$\boldsymbol{F}_{1\mu} = -\sum_{\boldsymbol{q}_\parallel} \boldsymbol{q}_\parallel \eta_\mu |U(\boldsymbol{q}_\parallel)|^2 \sum_{n=-\infty}^{\infty} [J_n^2(\xi)]'\Pi_1(\boldsymbol{q}_\parallel, \omega_0 - n\omega) - \sum_{\boldsymbol{q},\lambda} \boldsymbol{q}_\parallel \eta_\mu |M(\boldsymbol{q}, \lambda)|^2 \sum_{n=-\infty}^{\infty} [J_n^2(\xi)]'\Lambda_1(\boldsymbol{q}, \lambda, \omega_0 + \Omega_{\boldsymbol{q}\lambda} - n\omega), \tag{22}$$

$$\boldsymbol{F}_{2\mu} = \sum_{\boldsymbol{q}_\parallel} \boldsymbol{q}_\parallel \frac{\eta_\mu}{\xi} |U(\boldsymbol{q}_\parallel)|^2 \sum_{n=-\infty}^{\infty} 2nJ_n^2(\xi)\Pi_2(\boldsymbol{q}_\parallel, \omega_0 - n\omega) + \sum_{\boldsymbol{q},\lambda} \boldsymbol{q}_\parallel \frac{\eta_\mu}{\xi} |M(\boldsymbol{q}, \lambda)|^2 \sum_{n=-\infty}^{\infty} 2nJ_n^2(\xi)\Lambda_2(\boldsymbol{q}, \lambda, \omega_0 + \Omega_{\boldsymbol{q}\lambda} - n\omega). \tag{23}$$

In these expressions, $\eta_\mu \equiv \boldsymbol{q}_\parallel \cdot \boldsymbol{v}_\mu/\omega\xi$; $\omega_0 \equiv \boldsymbol{q}_\parallel \cdot \boldsymbol{v}_0$; $U(\boldsymbol{q}_\parallel)$ is related to the impurity potential $U(\boldsymbol{q}_\parallel, z_a)$ and distribution of impurities along the z-axis $n_i(z)$ [11]; $\Lambda_2(\boldsymbol{q}, \lambda, \Omega)$ is the imaginary part of the electron–phonon correlation function, which can be expressed through the imaginary part of the electron density correlation function $\Pi_2(\boldsymbol{q}_\parallel, \Omega)$ as [15]

$$\Lambda_2(\boldsymbol{q}, \lambda, \Omega) = 2\Pi_2(\boldsymbol{q}_\parallel, \Omega)\left[n\left(\frac{\Omega_{q\lambda}}{T}\right) - n\left(\frac{\Omega}{T_e}\right)\right], \tag{24}$$

with $n(x) \equiv 1/[\exp(x) - 1]$ being the Bose function. The real parts of the electron–phonon correlation function and the electron density correlation function, $\Lambda_1(\boldsymbol{q}, \lambda, \Omega)$ and $\Pi_1(\boldsymbol{q}_\parallel, \Omega)$, can be obtained from their imaginary parts through Kramers–Kronig transformation [15].

The momentum-balance equation, obtained by taking the statistical average of the operator equation (14), has the following form:

$$\boldsymbol{v}_1\omega\sin(\omega t) - \boldsymbol{v}_2\omega\cos(\omega t) = \frac{1}{N_e m}\boldsymbol{F}(t) + \frac{e}{m}\{\boldsymbol{E}_0 + \boldsymbol{E}(t) + [\boldsymbol{v}_0 + \boldsymbol{v}(t)] \times \boldsymbol{B}\}. \tag{25}$$

That is

$$0 = N_e e\boldsymbol{E}_0 + N_e e(\boldsymbol{v}_0 \times \boldsymbol{B}) + \boldsymbol{F}_0, \tag{26}$$

$$\boldsymbol{v}_1 = \frac{e\boldsymbol{E}_s}{m\omega} - \frac{1}{N_e m\omega}(\boldsymbol{F}_{11} - \boldsymbol{F}_{22}) - \frac{e}{m\omega}(\boldsymbol{v}_2 \times \boldsymbol{B}), \tag{27}$$

$$-\boldsymbol{v}_2 = \frac{e\boldsymbol{E}_c}{m\omega} + \frac{1}{N_e m\omega}(\boldsymbol{F}_{12} + \boldsymbol{F}_{21}) - \frac{e}{m\omega}(\boldsymbol{v}_1 \times \boldsymbol{B}). \tag{28}$$

The energy-balance equation is obtained by taking the long-time average of the statistically averaged operator equation (16) to be

$$N_e e\boldsymbol{E}_0 \cdot \boldsymbol{v}_0 + S_p - W = 0. \tag{29}$$

Here W is the time-averaged rate of energy transfer from the electron system to the phonon system, whose expression can be obtained from the second term on the right side of equation (21) by replacing the $\boldsymbol{q}_\parallel$-factor with $\Omega_{\boldsymbol{q}\lambda}$. S_p is the time-averaged rate of electron energy gain from the radiation field and has the following form:

$$S_p = \sum_{\boldsymbol{q}_\parallel} |U(\boldsymbol{q}_\parallel)|^2 \sum_{n=-\infty}^{\infty} n\omega J_n^2(\xi)\Pi_2(\boldsymbol{q}_\parallel, \omega_0 - n\omega) + \sum_{\boldsymbol{q},\lambda} |M(\boldsymbol{q},\lambda)|^2 \sum_{n=-\infty}^{\infty} n\omega J_n^2(\xi)\Lambda_2(\boldsymbol{q},\lambda, \omega_0 + \Omega_{\boldsymbol{q}\lambda} - n\omega). \tag{30}$$

Note that S_p is negatively equal to the time-averaged Joule heat $\langle \boldsymbol{v}(t)\cdot\boldsymbol{F}(t)\rangle_t = N_e e(\boldsymbol{E}_s \cdot \boldsymbol{v}_2/2 + \boldsymbol{E}_c \cdot \boldsymbol{v}_1/2)$.

The momentum- and energy-balance equations (26)–(29) constitute a closed set of equations for determining the parameters $\boldsymbol{v}_0$, $\boldsymbol{v}_1$, $\boldsymbol{v}_2$, and T_e when $\boldsymbol{E}_0$, $\boldsymbol{E}_c$, and $\boldsymbol{E}_s$ are given.

The sum over n in the expressions for $\boldsymbol{F}_0$, $\boldsymbol{F}_{\mu\nu}$, W, and S_p represents contribution of all orders of multiphoton processes related to the photons of frequency ω. In the present formulation, the role of the single-frequency radiation field is twofold:

(1) It induces photon-assisted impurity and phonon scatterings associated with single-photon ($|n| = 1$) and multiple-photon ($|n| \geqslant 1$) processes, which are superposed on the direct impurity and phonon scattering ($n = 0$) term.
(2) It transfers energy to the electron system (S_p) through single- and multiple-photon-assisted processes.

Note that $\Pi_2(\boldsymbol{q}_\parallel, \Omega)$ and $\Pi_1(\boldsymbol{q}_\parallel, \Omega)$ are respectively the imaginary and real parts of the electron density correlation function of the 2D system in the presence of the magnetic field. In the Landau representation, one can write [2]

$$\Pi_2(\boldsymbol{q}_\parallel, \Omega) = \frac{1}{2\pi l^2} \sum_{n,n'} C_{n,n'}(l^2 q_\parallel^2/2)\Pi_2(n, n', \Omega), \tag{31}$$

$$\Pi_2(n, n', \Omega) = -\frac{2}{\pi} \int \mathrm{d}\varepsilon\, [f(\varepsilon) - f(\varepsilon + \Omega)]\, \mathrm{Im}\, G_n^r(\varepsilon + \Omega)\, \mathrm{Im}\, G_{n'}^r(\varepsilon), \tag{32}$$

where $l = \sqrt{1/|eB|}$ is the magnetic length,

$$C_{n,n+l}(Y) = \frac{n!}{(n+l)!} Y^l \mathrm{e}^{-Y} [L_n^l(Y)]^2 \tag{33}$$

with $L_n^l(Y)$ being the associate Laguerre polynomial, $f(\varepsilon) = \{\exp[(\varepsilon - \mu)/T_e] + 1\}^{-1}$ the Fermi distribution function, and $\mathrm{Im}\, G_n^r(\varepsilon)$ the imaginary part of the Green function of the Landau level n, which is proportional to the density of states, such that the density of electrons is given by

$$N_e = -\frac{1}{\pi^2 l^2} \sum_n \int \mathrm{d}\varepsilon\, f(\varepsilon)\, \mathrm{Im}\, G_n^r(\varepsilon). \tag{34}$$

This equation determines the chemical potential.

In principle, to obtain the Green function of Landau levels n, $G_n^r(t)$, a self-consistent calculation has to be carried out based on the Dyson equation for the self-energy with all the scattering mechanisms included [16]. The resultant Green function is generally a complicated function of the magnetic field, temperature, and Landau-level index n, also dependent on the relative strength of the impurity and phonon scattering. In the present study we do not attempt

a self-consistent calculation of $G_n^r(t)$. Instead, we choose a Gaussian-type function for the Landau-level shape for simplicity [17]:

$$\mathrm{G}_n^r(t) = -\mathrm{i}\Theta(t)\exp[-\mathrm{i}(n-\tfrac{1}{2})\omega_c t - \tfrac{1}{2}\Gamma_n^2 t^2] \tag{35}$$

with a unified broadening parameter $\Gamma_n = \Gamma$ for all the Landau levels, which is taken as $(2e\omega_c/\pi m\mu_0)^{1/2}$. When the hot-electron effect is neglected, μ_0 corresponds to the linear mobility at temperature T in the absence of magnetic fields [18]. In order to consider the hot-electron-induced Landau-level broadening, we will empirically treat μ_0 as the linear mobility of the system in the absence of the magnetic field at temperature T_e. Note that this Gaussian-type Green function is proved to be correct at low temperature [19]. On the other hand, it has also been used to interpret the magnetophonon resonance at high lattice temperature [20]. In the present paper we will show that this Green function can lead to a qualitative agreement between theoretical and experimental results within the magnetic field range considered. To improve the agreement further, a more careful study on the Green function of a Landau level should be performed [16].

The above formulation can be used to describe the transport and optical properties of magnetically biased quasi-2D semiconductors subjected to a dc field and a THz field. The conventional magneto-optical study in the far-infrared frequency regime corresponds to the case of zero dc field $\boldsymbol{E}_0 = 0$, where one studies the intensity-dependent THz absorption, transmission, and other effects in the presence of a strong magnetic field. On the other hand, to investigate photoconductivity, we should treat the limit for weak dc field of our formulation.

3. Cyclotron resonance in drift velocity

Substituting the force equation (27) into (28), we can write

$$\boldsymbol{v}_1 = (1-\omega_c^2/\omega^2)^{-1}\left\{\frac{e}{m\omega}\left[\boldsymbol{E}_s + \frac{e}{m\omega}(\boldsymbol{E}_c\times\boldsymbol{B})\right] - \frac{1}{N_e m\omega}\left(\boldsymbol{F}_{11} - \boldsymbol{F}_{22} - \frac{e}{m\omega}[(\boldsymbol{F}_{12}+\boldsymbol{F}_{21})\times\boldsymbol{B}]\right)\right\}, \tag{36}$$

$$-\boldsymbol{v}_2 = (1-\omega_c^2/\omega^2)^{-1}\left\{\frac{e}{m\omega}\left[\boldsymbol{E}_c - \frac{e}{m\omega}(\boldsymbol{E}_s\times\boldsymbol{B})\right] + \frac{1}{N_e m\omega}\left(\boldsymbol{F}_{12} + \boldsymbol{F}_{21} + \frac{e}{m\omega}[(\boldsymbol{F}_{11}-\boldsymbol{F}_{22})\times\boldsymbol{B}]\right)\right\}. \tag{37}$$

CR is easily seen in the case of weak scatterings when the terms with $\boldsymbol{F}_{\mu\nu}$-functions in the above equation are small: both $\boldsymbol{v}_1$ and $\boldsymbol{v}_2$ exhibit peaks at CR. Since all the transport quantities, including W, S_p, and $\boldsymbol{F}_0$, are functions of the drift velocity as well as the electron temperature T_e, and the latter is determined by the energy-balance equation (30), the CR of $\boldsymbol{v}_1$ and $\boldsymbol{v}_2$ will result in CR in W, S_p, $\boldsymbol{F}_0$, and T_e.

Equations (36) and (37) can be further simplified when the radiation field is weak and the dc field is absent. In this case the $\boldsymbol{v}_\mu$ can be treated as small parameters. To the first order of these small parameters, the force function $\boldsymbol{F}_{\mu\nu}$ can be written as

$$\boldsymbol{F}_{\mu\nu} = N_e m\boldsymbol{v}_\nu M_\mu(\omega, \boldsymbol{v}_0) \qquad (\mu, \nu = 1, 2), \tag{38}$$

where $M_\mu(\omega, \boldsymbol{v}_0)$ are the real ($\mu = 1$) and imaginary ($\mu = 2$) parts of the memory functions [15]. It is convenient to write out the expression for the complex velocity

$v_+ \equiv v_{1x} + \mathrm{i}v_{2x}$ and $v_- \equiv v_{2y} - \mathrm{i}v_{1y}$ rather than for $\boldsymbol{v}_1$ and $\boldsymbol{v}_2$:

$$\begin{aligned} v_+ &= (e\tau/2m^*)\left(\frac{E_+}{(\omega-\omega_c^*)\tau+\mathrm{i}} + \frac{E_-}{(\omega+\omega_c^*)\tau+\mathrm{i}}\right), \\ v_- &= -(e\tau/2m^*)\left(\frac{E_+}{(\omega-\omega_c^*)\tau+\mathrm{i}} - \frac{E_-}{(\omega+\omega_c^*)\tau+\mathrm{i}}\right). \end{aligned} \tag{39}$$

Here, we have defined

$$\begin{aligned} m^* &= m[1 + M_1(\omega, \boldsymbol{v}_0)/\omega], \\ 1/\tau &= M_2(\omega, \boldsymbol{v}_0)/[1 + M_1(\omega, \boldsymbol{v}_0)/\omega], \\ \omega_c^* &= eB/m^*, \\ E_+ &= E_{sx} + E_{cy} + \mathrm{i}(E_{sy} - E_{cx}), \\ E_- &= E_{sx} - E_{cy} - \mathrm{i}(E_{sy} + E_{cx}), \end{aligned}$$

with $(E_{sx}, E_{sy}) \equiv \boldsymbol{E}_s$ and $(E_{cx}, E_{cy}) \equiv \boldsymbol{E}_c$.

Our weak-field results for $\boldsymbol{v}_1$ and $\boldsymbol{v}_2$ reduce to those of [2] in the case of circularly polarized ac fields.

4. Transmission

For normally incident electromagnetic waves, the transmitted electric field $\boldsymbol{E}(t)$, which is regarded as the field driving the 2D electrons [21], is related to the incident electric field $\boldsymbol{E}_i(t)$ by

$$\boldsymbol{E}(t) = \frac{N_e e\boldsymbol{v}(t)/\epsilon_0 c}{n_s + n_0} + \frac{2n_0}{n_s + n_0}\boldsymbol{E}_i(t). \tag{40}$$

Here n_0 and n_s are the relative refractive indices of the air and 2D semiconductors, and c and ϵ_0 are the light speed and the dielectric constant in vacuum, respectively. The transmitted field $\boldsymbol{E}(t)$ depends on the drift velocity $\boldsymbol{v}(t)$ of the 2D system. In the following numerical studies on transmission and photoconductivity, we will assume a sinusoidal incident field $\boldsymbol{E}_i(t) = (E_{is}\sin(\omega t), 0)$ along the x-axis and derive $\boldsymbol{E}(t)$ self-consistently together with $\boldsymbol{v}(t)$.

We have numerically calculated the magneto-optical properties of a GaAs/AlGaAs heterojunction subjected to a THz ac field and a magnetic field. The strength of the transmitted ac field $\boldsymbol{E}(t)$, and the parameters $\boldsymbol{v}_\mu$ ($\mu = 1, 2$) and T_e, are obtained by resolving the equations (40), (27)–(29). We consider a GaAs-based quasi-2D system having electron density $N_e = 2.5 \times 10^{15}$ m^{-2} and 4.2 K linear mobility 50 m^2 V^{-1} s^{-1} (which is used to determine the impurity density) at lattice temperature $T = 4.2$ K, similar to that used in [3]. The elastic scattering due to randomly distributed charged impurity and the inelastic scattering due to polar optical phonons (via Fröhlich coupling with electrons), longitudinal acoustic phonons (via deformation potential and piezoelectric coupling), and transverse acoustic phonons (via piezoelectric coupling with electrons) are taken into account. The material and electron–phonon coupling parameters are taken as values typical for GaAs. In the numerical calculation the maximum Landau level is taken to be 20, and the summations over multiphoton indices n are carried out up to a given accuracy of 10^{-3} for each quantity.

The transmittance $\mathcal{T}$ can be defined as [21]

$$\mathcal{T} = \frac{\langle|\boldsymbol{E}(t)|^2\rangle_t}{\langle|\boldsymbol{E}_i(t)|^2\rangle_t} \tag{41}$$

with $\langle\cdot\rangle_t$ denoting the time average. When connecting it with measured quantities, of course, the multiple interference effect between interfaces of the substrate has to be taken into

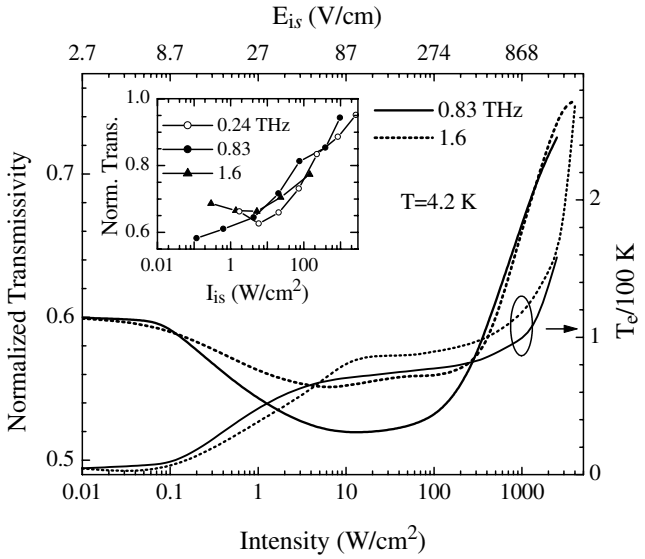

Figure 1. The intensity dependence of the 2D semiconductor transmittance and electron temperature is plotted at the CR position, $\omega_c = \omega$. The transmittance is normalized to the value for zero magnetic field. THz fields with two different frequencies $\omega/2\pi = 0.83$ and 1.6 THz are exerted on the 2D system studied. The lattice temperature is $T = 4.2$ K. Experimental results for transmittance versus the intensity of the THz fields I_{is} (figure 2 of [3]) are reproduced in the inset.

account. The calculated transmittance and the corresponding electron temperature are plotted in figure 1 as functions of the intensity of the THz field at two frequencies $\omega/2\pi = 0.83$ and 1.6 THz in the centre position of the CR, namely $\omega_c = \omega$. It can be seen that the transmittance first decreases gently with increasing intensity of the THz radiation from zero, and reaches a minimum at a critical intensity around 10 W cm^{-2}, then increases rapidly with further increasing field strength. This feature appears more pronounced at lower frequency, consistently with the experimental observation [3], as shown in the inset of figure 1, where the measured transmittance for 1.6 and 0.24 THz exhibits a similar trend. The case of 0.83 THz does not show a minimum. This deviation is believed to come from the experimental errors. In figure 2 we display the transmittance CR line shape for incident electromagnetic fields of different intensities at frequency 0.83 THz. The linewidth exhibits no significant change below the critical intensity but increases rapidly when the intensity of THz field grows above the critical value.

This kind of E_{is}-dependent behaviour of the transmittance is in agreement with the intensity dependence of the absorption rate $\alpha \sim S_p/E_{is}^2$ in the absence of the magnetic field. For a similar 2D GaAs-based semiconductor without a magnetic field, we [9] showed that the absorption percentage increases with increasing strength of the radiation field from the low-field value, then reaches a maximum (of the order of 2%) at a field amplitude around several kilovolts per centimetre, before decreasing with further increase of the radiation field strength, and that for lower frequency there is a stronger maximum. On the low-velocity side, when the hot-electron effect is relatively weak and the direct impurity and phonon scatterings change little, the behaviour of the absorption rate comes mainly from the drift velocity dependence of the multiphoton-assisted scattering matrix element, as described by the Bessel functions $J_n^2(\xi)$ in the expressions for S_p. In fact, all the multiphoton ($n \geqslant 1$) contributions to the absorption coefficient are zero at vanishing velocity and reach maxima at finite (increasing with n) drift velocities; the resultant absorption coefficient at first increases with increasing velocity. When

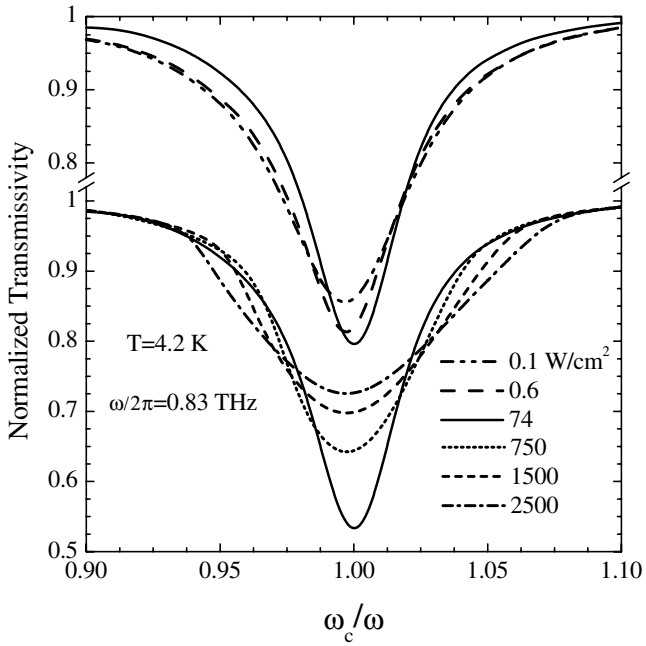

Figure 2. The CR of the 2D semiconductor transmittance for several incident electromagnetic fields with a same frequency $\omega/2\pi = 0.83$ THz but different intensities $I_{is} = 0.1$, 0.6, 74, 750, 1500, 2500 W cm^{-2}.

the drift velocity becomes sufficiently large, the reduction of absorption rates, induced by the large argument of the lowest-order Bessel functions, will exceed the increased contributions from the other multiphoton processes. This leads to a drop of the absorption rate. In the present case, having a strong magnetic field, the CR greatly enhances the drift velocity $\boldsymbol{v}_1$ and $\boldsymbol{v}_2$ at $\omega_c \sim \omega$ for a given E_{is} in comparison with the case without a magnetic field. Therefore, the maximum absorption rate should appear at much smaller strength of the radiation field and a have much larger value for the case of CR than in the absence of a magnetic field or far away from CR.

The behaviour of the transmittance CR line shape is related to Landau-level broadening due to hot-electron effects. For a THz field below the critical intensity the electron temperature is less than 60 K (see figure 1) and impurities are the dominant scatterers, yielding an almost constant mobility μ_0 (and thus the Landau-level broadening). When the THz field goes above the critical intensity, the electron temperature grows rapidly, and polar optical phonons become the dominant scatterers, giving rise to a strongly temperature-dependent mobility μ_0, and thus a Landau-level broadening which increases rapidly with increasing field strength.

Our formulation can also be employed to investigate the change of the transmitted electromagnetic field polarization in quasi-two-dimensional electron systems. This effect is known as the Faraday effect and it has long been investigated under linear conditions [22–24]. The present approach provides a convenient formulation for studying the Faraday effect for the case where the incident light is strong and nonlinear absorption occurs.

The relevant quantities characterizing the Faraday effects are the ellipticity η and Faraday rotation angle θ_F, which are determined through the amplitudes of the transmitted field $\boldsymbol{E}(t)$:

$$\tan\eta = (a^+ - a^-)/(a^+ + a^-), \tag{42}$$

$$\theta_F = (\phi^+ - \phi^-)/2, \tag{43}$$

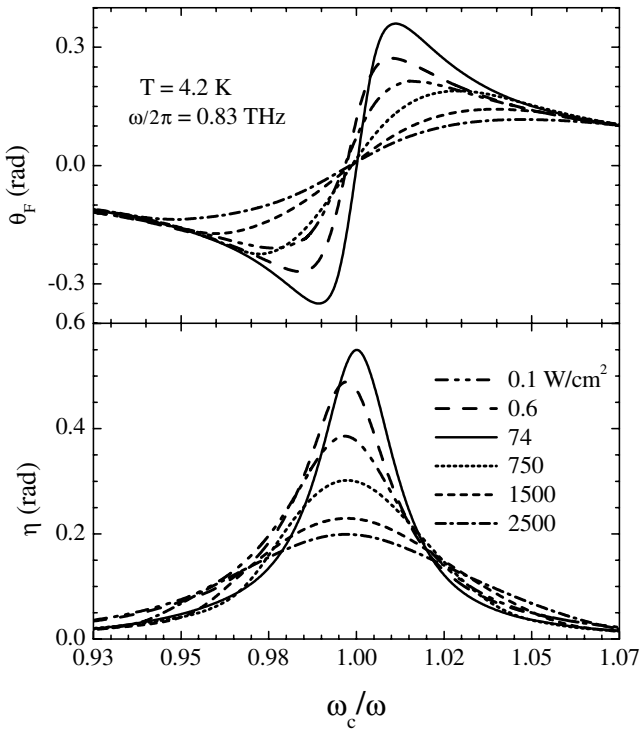

Figure 3. The Faraday angle θ_F and ellipticity η are plotted as functions of the strength of the magnetic field B for the same system and under the same conditions as for figure 2.

where

$$\tan\phi^+ = \frac{E_{sx} + E_{cy}}{E_{cx} - E_{sy}}, \tag{44}$$

$$\tan\phi^- = \frac{-E_{sx} + E_{cy}}{E_{cx} + E_{sy}}, \tag{45}$$

$$a^+ = \sqrt{(E_{sx} + E_{cy})^2 + (E_{cx} - E_{sy})^2}/2, \tag{46}$$

$$a^- = \sqrt{(E_{sx} - E_{cy})^2 + (E_{cx} + E_{sy})^2}/2, \tag{47}$$

with $(E_{sx}, E_{sy}) \equiv \boldsymbol{E}_s$ and $(E_{cx}, E_{cy}) \equiv \boldsymbol{E}_c$.

We plot the calculated results for η and θ_F in figure 3 for the above-mentioned two-dimensional sample. The resonance in ellipticity and antiresonance in the Faraday angle can be seen clearly. Their line shapes also manifest different behaviours when the intensity of THz field lies below or above the critical value. These intensity-dependent behaviours of the ellipticity and Faraday rotation can also be understood on the basis of multiphoton-assisted scatterings and hot-electron-effect-induced Landau-level broadening.

5. Photoconductivity

The response of the linear dc conductance to far-infrared irradiation is easily obtained in the limit of weak dc field for our formulation. Taking $\boldsymbol{v}_0$ to be in the x-direction, $\boldsymbol{v}_0 = (v_{0x}, 0, 0)$,

and expanding equation (26) to the first order in v_{0x}, we obtain the transverse and longitudinal resistivities R_{xy} and R_{xx} as follows:

$$R_{xy} \equiv \frac{E_{0y}}{N_e e v_{0x}} = B/N_e e, \tag{48}$$

$$R_{xx} \equiv \frac{E_{0x}}{N_e e v_{0x}} = -\frac{1}{N_e^2 e^2} \sum_{\boldsymbol{q}_\parallel} q_x^2 |U(\boldsymbol{q}_\parallel)|^2 \sum_{n=-\infty}^{\infty} J_n^2(\xi) \left[\frac{\partial}{\partial \Omega} \Pi_2(\boldsymbol{q}_\parallel, \Omega) \right]_{\Omega=-n\omega}$$
$$- \frac{1}{N_e^2 e^2} \sum_{\boldsymbol{q},\lambda} q_x^2 |M(\boldsymbol{q}, \lambda)|^2 \sum_{n=-\infty}^{\infty} J_n^2(\xi) \left[\frac{\partial}{\partial \Omega} \Lambda_2(\boldsymbol{q}, \lambda, \Omega) \right]_{\Omega=\Omega_{q\lambda}-n\omega}. \tag{49}$$

The parameters $\boldsymbol{v}_1$, $\boldsymbol{v}_2$, and T_e in these expressions should be determined by solving equations (27)–(29) with zero $\boldsymbol{v}_0$. The longitudinal photoresistivity is defined as

$$\Delta R_{xx} \equiv R_{xx} - R_{xx}^0, \tag{50}$$

with R_{xx}^0 being the longitudinal magnetoresistivity in the absence of the radiation field.

Photoconductivity in semiconductors, in the absence or in the presence of magnetic fields, has long been known at low temperatures, and was understood to result from the effects of electron heating due to the absorption of the radiation field energy [5, 25, 26]. In our formulation, the photoconductivity arises not only from the hot-electron effect (electron temperature change), but also from photon-assisted electron–impurity and electron–phonon scatterings. Although it is difficult to distinguish contributions to photoconductivity from different mechanisms when the applied THz field is strong, in the case of weak ac fields, the longitudinal photoresistivity can be written as the sum of two terms:

$$\Delta R_{xx} = \Delta R_{xx}^{(h)} + \Delta R_{xx}^{(op)}. \tag{51}$$

The first term $\Delta R_{xx}^{(h)}$ is obtained through expanding equation (49) in the small parameter $\Delta T_e = T_e - T$ and is the result of ac-field-induced electron temperature change, like that proposed first by Kogan for the case without a magnetic field [25]. After determining the small electron temperature change from the energy-balance equation (29), we can write

$$\Delta R_{xx}^{(h)} = \Phi \, \Delta T_e. \tag{52}$$

Here

$$\Phi \equiv \left(\frac{\partial R_{xx}^0}{\partial T_e} \right)_{T_e=T} = \frac{\partial}{\partial T} R_{xx}^0 - \frac{2}{N_e^2 e^2} \sum_{\boldsymbol{q},\lambda} q_x^2 |M(\boldsymbol{q}, \lambda)|^2$$
$$\times \frac{\Omega_{q\lambda}}{T^2} n' \left(\frac{\Omega_{q\lambda}}{T} \right) \left[\frac{\partial}{\partial \Omega} \Pi_2(\boldsymbol{q}_\parallel, \Omega) \right]_{\Omega=\Omega_{q\lambda}}, \tag{53}$$

and

$$\Delta T_e = \Xi \left[8 \sum_{\boldsymbol{q},\lambda} \frac{\Omega_{q\lambda}^2}{T^2} |M(\boldsymbol{q}, \lambda)|^2 \Pi_2(\boldsymbol{q}_\parallel, \Omega_{q\lambda}) n' \left(\frac{\Omega_{q\lambda}}{T} \right) \right]^{-1}, \tag{54}$$

with

$$\Xi = \frac{1}{\omega^2} (\boldsymbol{v}_1^2 + \boldsymbol{v}_2^2) \left[N_e m \omega M_2(\omega, 0) - \sum_{\boldsymbol{q},\lambda,\pm} \Omega_{q\lambda} q_\parallel^2 |M(\boldsymbol{q}, \lambda)|^2 \Lambda_2(\boldsymbol{q}_\parallel, \Omega_{q\lambda} \pm \omega) \right]. \tag{55}$$

Note that the terms on the right-hand side of equation (55) are respectively the changes of S_p and W induced by photon-assisted scatterings.

The second component of the photoresistivity $\Delta R_{xx}^{(op)}$ is the result of the photon-assisted scattering processes and ac-field-induced electron distribution change

$$\Delta R_{xx}^{(op)} = \frac{1}{4N_e^2 e^2 \omega}(3v_{1x}^2 + 3v_{2x}^2 + v_{1y}^2 + v_{2y}^2)Q_2(\omega) \tag{56}$$

where

$$Q_2(\omega) = \sum_{q_\parallel} q_\parallel^4 [A_d(\boldsymbol{q}_\parallel, 0) - A_d(\boldsymbol{q}_\parallel, \omega)]/\omega, \tag{57}$$

with

$$A_d(\boldsymbol{q}_\parallel, \Omega) = |U(\boldsymbol{q}_\parallel)|^2 \frac{\partial}{\partial \Omega}\Pi_2(\boldsymbol{q}_\parallel, \Omega) + \sum_{q_z,\lambda} |M(\boldsymbol{q}, \lambda)|^2 \frac{\partial}{\partial \Omega}\Lambda_2(\boldsymbol{q}, \lambda, \Omega). \tag{58}$$

In the weak-ac-field limit we can see from equation (39) that the amplitudes of the time-dependent drift velocity are linearly dependent on the strength of the applied THz fields. Consequently, the photoresistivity is proportional to the intensity of the THz field. When the intensity of the driving field becomes strong, the dependence of the photoconductivity on the strength of the THz field exhibits a complicated behaviour. At the same time, the contribution from the electron temperature change and nonthermal photon-assisted scattering are hybridized. At low lattice temperatures, the hot-electron effect is sufficiently strong and is generally the dominant mechanism for photoresistivity. At high temperature, however, when the polar optical phonon scattering provides an efficient energy dissipation channel, the photoconductivity is mainly contributed from nonthermal mechanisms.

Recently, the photoconductivity CR at high temperature has been demonstrated in the experiment of [7]. Remarkable peaks in the photoconductivity are observed when the cyclotron frequency is close to the frequency of the THz fields. It is also found that not only the heights but also the widths of CR peaks increase with increasing intensity of the THz fields.

In order to illustrate CR in photoconductivity at high lattice temperatures, we have numerically evaluated the dc longitudinal photoresistivity of a magnetically biased GaAs/AlGaAs heterojunction. The lattice temperature T is 150 K. The sample considered has electron density $N_e = 2.0 \times 10^{15}$ m^{-2} and 4.2 K linear mobility 200 m^2 V^{-1} s^{-1}, similar to that in the experiment of [7].

In figure 4 the longitudinal photoresistivity induced by THz fields of frequency $\omega/2\pi =$ 4 THz having several different amplitudes is plotted as a function of magnetic field. The resonant structure near the CR position shows up clearly. Furthermore, with increasing strength of the THz field, the CR peaks ascend and the line shapes broaden. These features are in qualitative agreement with the experimental results in [7]. In the inset of figure 4 we plot the photoresistivity at CR as a function of the intensity of the THz field. One can see that the photoresistivity follows a linear dependence on the intensity of the THz field in the range $0 < I_{is} < 1$ kW cm^{-2}. For larger ac field intensity, the deviation from linear dependence appears. The electron temperature also exhibits a resonant peak when the cyclotron frequency is close to the THz frequency, as shown in figure 5. Nevertheless, since at high lattice temperatures the strong electron–LO phonon scattering provides an efficient energy dissipation channel, the rise of the electron temperature is modest, and the hot-electron-effect-induced photoconductivity is small in comparison with the nonthermal effect. The photon-assisted scatterings are the main mechanisms for the photoconductivity at high temperature. For relatively weak radiation fields, e.g. $E_{is} \leqslant 0.24$ kV cm^{-1}, the electron temperature has no appreciable difference from T, yet ΔR_{xx} still exhibits sizable resonance, comparable with the peak height observed in experiments of [7]. In figure 6 we plot the longitudinal photoresistivity as a function of magnetic field strength for relatively weak ac fields. The contribution to the

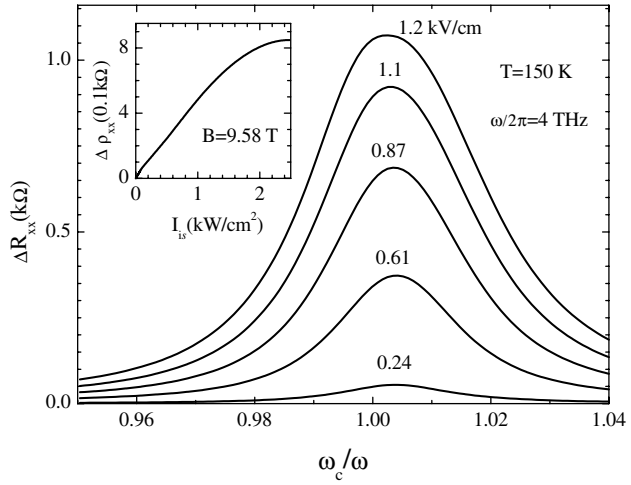

Figure 4. The CR in the longitudinal resistivity change ΔR_{xx} induced by a radiation field of frequency $\omega/2\pi = 4$ THz having several different amplitudes $E_{is} = 0.24$, 0.61, 0.87, 1.1, 1.2 kV cm^{-1}. The lattice temperature is $T = 150$ K. The inset shows ΔR_{xx} versus intensity for incident THz fields I_{is} at $\omega_c = \omega$.

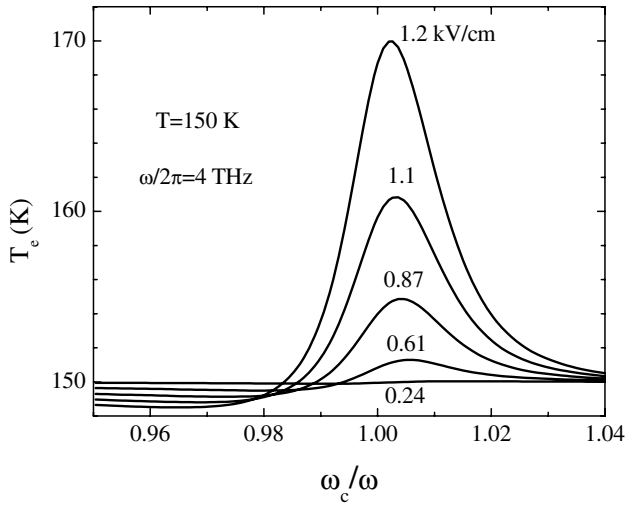

Figure 5. The CR in the electron temperature T_e for the same system and under the same conditions as for figure 4.

photoconductivity from the hot-electron effect is less than 3%. We also show the experimental observation [7] of CR in photoconductivity in the inset of figure 6. The extraordinary width of the resonance shown in the experimental ΔR_{xx} is possible due to the small pulse extent or large bandwidth of the THz radiation used in the experiment, as explained in [7].

6. Conclusions

We have developed the momentum- and energy-balance equations for steady-state electron transport and optical absorption under the influence of a dc electric field and an intense THz

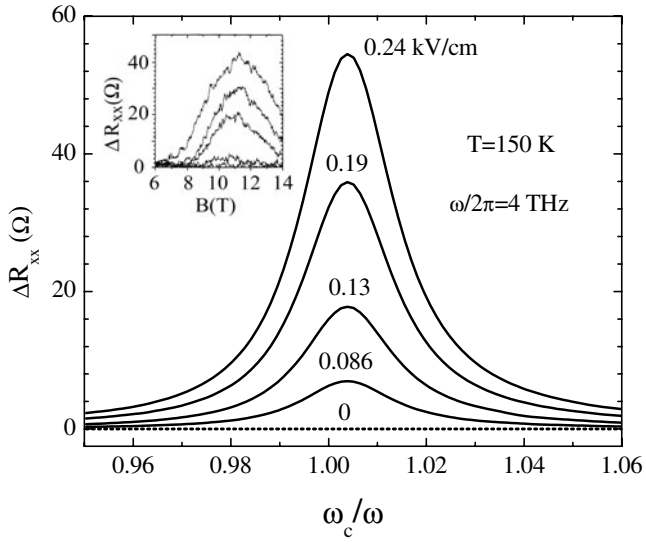

Figure 6. Similar to figure 4, but the strengths of THz fields are relatively low: $E_{is} = 0$, 0.086, 0.13, 0.19, 0.24 kV cm^{-1}. The experimental results (figure 3 of [7]) on the CR in photoconductivity are shown in the inset.

ac electric field in a two-dimensional semiconductor in the presence of a strong magnetic field perpendicular to the 2D plane. This formulation allows us to investigate the THz field intensity dependence of the CR in the transmittance and photoconductivity of GaAs/AlGaAs heterojunctions. We found that the CR peaks and line shapes of the transmittance exhibit different behaviours when the intensity of the THz field increases in the ranges above or below a certain critical value. The CR in the photoresistivity, however, is always enhanced with increased intensity of the THz field. These results qualitatively agree with the experimental observations. The intensity-dependent behaviour of the transmittance at CR is explained as the result of combing hot-electron-effect-induced Landau-level broadening and electron–phonon scattering enhancement, and the drift velocity dependence of the photon-assisted scattering matrix elements. We have also clarified that the CR in the photoconductivity is not only a result of the electron heating but also arises from photon-assisted scattering enhancement, especially at high temperatures. The effects of an intense THz field on the Faraday angle and ellipticity of magnetically biased 2D semiconductor systems have also been demonstrated.

Acknowledgments

The authors gratefully acknowledge stimulating discussions with Drs Bing Dong and W S Liu. This work was supported by the National Science Foundation of China (Grant Nos 60076011 and 90103027), the Special Funds for Major State Basic Research Project (Grant No 20000683), the Shanghai Municipal Commission of Science and Technology, and the Shanghai Postdoctoral Fellow Science Foundation.

References

[1] Kono J, Chin A H, Mitchell A P, Takahashi T and Akiyama H 1999 *Appl. Phys. Lett.* **75** 1119
Khodaparast G A, Larrabee D C, Kono J, King D S, Chung S J and Santos M B 2003 *Phys. Rev.* B **67** 035307
[2] Ting C S, Ying S C and Quinn J J 1977 *Phys. Rev.* B **16** 5394

[3] Rodriguez G A, Hart R M, Sievers A J, Keilmann F, Schlesinger Z, Wright S L and Wang W I 1986 *Appl. Phys. Lett.* **49** 458
[4] Maan J C, Englert Th and Tsui D C 1982 *Appl. Phys. Lett.* **40** 609
[5] Hirakawa K, Yamanaka K, Kawaguchi Y, Endo M, Saeki M and Komiyama S 2001 *Phys. Rev.* B **63** 085320
Kawaguchi Y, Hirakawa K, Saeki M, Yamanaka K and Komiyama S 2002 *Appl. Phys. Lett.* **80** 136
[6] Mordovets N A and Kotel'nikov I N 1994 *Semiconductors* **28** 1080
[7] Koenraad P M, Lewis R A, Waumans L R C, Langerak C J G M, Xu W and Wolter J H 1998 *Physica* B **256–268** 268
[8] Lei X L 1998 *J. Appl. Phys.* **84** 1396
Lei X L 1998 *J. Phys.: Condens. Matter* **10** 3201
[9] Lei X L and Liu S Y 2000 *J. Phys.: Condens. Matter* **12** 4655
[10] Lei X L and Liu S Y 2000 *Eur. Phys. J.* B **13** 271
[11] Lei X L, Birman J L and Ting C S 1985 *J. Appl. Phys.* **58** 2270
[12] Lei X L and Ting C S 1985 *Phys. Rev.* B **32** 1112
[13] Mayer A and Keilmann F 1986 *Phys. Rev.* B **33** 6962
[14] Lei X L 1997 *J. Appl. Phys.* **82** 718
[15] Lei X L and Horing N J M 1992 *Int. J. Mod. Phys.* B **6** 805
[16] Leadley D R, Nicholas R J, Singleton J, Xu W, Peeters F M, Devreese J T, Perenboom J A A J, van Bockstal L, Herlach F, Harris J J and Foxon C T 1993 *Phys. Rev.* B **48** 5457
Leadley D R, Nicholas R J, Singleton J, Xu W, Peeters F M, Devreese J T, Perenboom J A A J, van Bockstal L, Herlach F, Harris J J and Foxon C T 1994 *Phys. Rev. Lett.* **73** 589
[17] Gerhardts R R 1975 *Z. Phys.* B **21** 275
[18] Ando T 1975 *J. Phys. Soc. Japan* **38** 989
[19] See, e.g.,
Gudmundsson V and Gerhardts R R 1987 *Phys. Rev.* B **35** 8005 and references therein
[20] Barnes D J, Nicholas R J, Peeters F M, Wu X-G, Devreese J T, Singleton J, Langerak C J G M, Harris J J and Foxon C T 1991 *Phys. Rev. Lett.* **66** 794
[21] Chiu K W, Lee T K and Quinn J J 1976 *Surf. Sci.* **58** 182
[22] For recent theoretical work, see, e.g.,
Popov V V and Teperik T V 1999 *JETP Lett.* **70** 254
[23] O'Connell R F and Wallace G 1982 *Phys. Rev.* B **26** 2231
[24] Volkov V A, Galchenkov D V, Galchenkov L A, Grodnenskii I M, Matov O R, Mikhailov S A, Senichkin A P and Starostin K V 1986 *JETP Lett.* **43** 326
[25] Kogan Sh M 1963 *Sov. Phys.–Solid State* **4** 1386
[26] Valov P M, Ryvkin B S, Yaroshetskii I D and Yassievich I N 1971 *Sov. Phys.–Semicond.* **5** 797